arXiv:hep-ph/9511220v1 3 Nov 1995

Mass or Gravitationally Induced Neutrino Oscillations? – A Comparison of ^8B Neutrino Flux Spectra in a Three–Generation Framework

J. R. Mureika* and R. B. Mann†

Department of Physics
University of Waterloo
Waterloo, Ontario N2L 3G1 Canada

February 1, 2008

Abstract

Both gravitational and mass induced neutrino oscillation mechanisms provide possible resolutions to the Solar Neutrino Problem. The distinguishing feature between the two mechanisms is their dependence on the neutrino energy. We investigate the implications of this by computing the ^8B neutrino spectrum as determined from each mechanism using a realistic three–flavor evolution model. We find that in the limit of small θ_{13} mixing angle, the differences are significant enough to observe in future solar neutrino experiments.

*newt@avatar.uwaterloo.ca
†mann@avatar.uwaterloo.ca

The Solar Neutrino Problem (SNP) has perplexed both astrophysicists and particle physicists for upwards of thirty years now. The measured flux of ν_es incident on the Earth–bound detectors [1, 2, 3, 4] remains in conflict with the standard solar model prediction (see [5] for a review). A plausible expanation of this discrepancy is that oscillations take place between electron neutrinos and neutrinos of differing species, thereby reducing the expected ν_e flux to an empirically acceptable value.

At present there are two qualitatively distinct mechanisms which could give rise to such oscillations. One is the well-known Mikayev–Smirnov–Wolfenstein (MSW) mechanism [6, 7, 8] which postulates that neutrinos possess a non–trivial mass eigenbasis, in contrast to the assumptions of the Minimal Standard Model. In this mechanism electron neutrinos produced at the core of the sun will, under certain conditions dependent upon the solar electron density, undergo a resonance with other species of neutrinos whose flux then has no effect on earth-based detectors. Another mechanism proposed more recently [9] hypothesizes that neutrinos posess a flavor–dependent coupling to the external gravitational field. This mechanism (recently dubbed the VEP mechanism [10]) violates the Einstein Equivalence Principle (EEP), since it requires $G_i = (1 + f_i)G$, where G is Newton's constant, i a flavor index, and f_i dimensionless parameters which characterize the degree of EEP violation, with each $f_i \ll 1$. To ensure the full effect of three flavors, we must have $f_i \neq f_j, i \neq j$. For first generation neutrinos, we define $f_1 = 0$, *i.e.* $G_1 = G$. The VEP mechanism does not require neutrinos to have a non-degenerate mass-matrix.

Both oscillation mechanisms rest on the assumption that the two neutrino eigenstates, flavor ($|\nu\rangle_W$) and mass/gravitational ($|\nu\rangle_{M,G}$), are related by an $SU(N_g)$ transformation,

$$|\nu\rangle_W = V_3 \, |\nu\rangle_{M,G} \ , \tag{1}$$

where $N_g = 3$ for three flavors. These states evolve according to the equation [9]

$$\begin{aligned} & i\tfrac{d}{dr} \, |\nu\rangle_{M,G} = H_{M,G} \, |\nu\rangle_{M,G} \\ \Longrightarrow \quad & i\tfrac{d}{dr} \, |\nu\rangle_W = \left\{ V_3^\dagger H_{M,G} V_3 + A(r) \right\} \, |\nu\rangle_W \ . \end{aligned} \tag{2}$$

Flavor oscillations and resonances arise due to the off–diagonality of the modified Hamiltonian $V_3^\dagger H_{M,G} V_3 + A(r)$, where $A(r) = diag(\sqrt{2} G_F N_E(r), 0, 0)$

is the term in the Hamiltonian corresponding to ν_e-e (*i.e.* charged–current) electroweak interactions. If we assume no CP–violation in the neutrino sector, then the four–parameter matrix V_3 reduces to a real, orthogonal rotation with three vacuum mixing angles θ_{12}, θ_{13}, and θ_{23}.

The main difference between the MSW and VEP mechanisms manifests itself in the energy dependence of the evolution equations in (2). which respectively are

$$H_M = \frac{1}{2E} \begin{pmatrix} m_1^2 & 0 & 0 \\ 0 & m_2^2 & 0 \\ 0 & 0 & m_3^2 \end{pmatrix} , \tag{3}$$

$$H_G = 2E|\phi| \begin{pmatrix} f_1 & 0 & 0 \\ 0 & f_2 & 0 \\ 0 & 0 & f_3 \end{pmatrix} , \tag{4}$$

where a factor of unity has been subtracted out in each of (4) and (4) as it contributes only an overall unobservable phase. We have taken this factor to be $\mathbb{1} \cdot (H_{M,G})_{11}$, leaving the dynamics of the mechanism dependent of the eigenvalue differences $\Delta m_{ij}^2 \equiv m_i^2 - m_j^2$, $\Delta f_{ij} \equiv f_i - f_j$.

In this paper we consider the effect of these differing energy dependences on the suppression of the ^8B neutrino flux in the three–generation scheme. We show that for a small $\nu_e \to \nu_\tau$ mixing angle θ_{13}, there is a noticeable energy dependence in the shape and size of the suppression curves for MSW and VEP. This could be easily detected in present–day and future water detectors. For large θ_{13}, the suppression is energy–independent, and hence there is little variation in the spectrum. We shall take $\phi \equiv \phi_\odot(r)$ in (4), where $\phi_\odot(r)$ is the solar gravitational potential[1].

In order to study the suppression of ν_es, we must determine the model–dependent survival probability for these neutrinos as they travel from the solar center to the Earth–based detectors. Averaged over 1 AU, the solution to (2) can be written [12]

$$\langle P(\nu_e \to \nu_e) \rangle = \sum_{i,j=1}^{3} |(V_3)_{1i}|^2 \, |(P_{LZ})_{ij}|^2 \, |(V_3^m)_{1j}|^2$$

[1]We do not consider the effects of ν_e–regeneration in the Earth (the "day–night effect"), nor do we consider the minimal contribution of the local supercluster. For discussions as to why these can be excluded, see [10], or [13].

$$
\begin{aligned}
= \; & c^2_{m12}c^2_{m13}\left\{(1-P_1)c^2_{12}c^2_{13}+P_1 s^2_{12}c^2_{13}\right\} \\
& +s^2_{m12}c^2_{m13}\left\{P_1(1-P_2)c^2_{12}c^2_{13}+(1-P_1)(1-P_2)s^2_{12}c^2_{13}+P_2 s^2_{13}\right\} \\
& +s^2_{m13}\left\{P_1P_2c^2_{12}c^2_{13}+P_2(1-P_1)s^2_{12}s^2_{13}+(1-P_2)s^2_{13}\right\} \; .
\end{aligned}
\tag{5}
$$

The terms

$$
s_{ij} \equiv \sin\theta_{ij} \; , \; c_{ij} \equiv \cos\theta_{ij} \tag{6}
$$

refer to the vacuum mixing angles, while s_{mij}, c_{mij} are the analogous matter–enhanced trigonometric functions [14]. The referenced work expresses the functions in terms of MSW parameters; for VEP, we make the global substitution

$$
\frac{dm_{ij}}{2E} \; \rightarrow \; 2E|\phi|\Delta f_{ij} \; . \tag{7}
$$

The functions P_i are the Landau–Zener jump probabilities [12] for non–adiabatic state transitions, and are inherently energy–dependent.

The matter–enhanced mixing angles θ^m_{1j} [14] are dependent upon the point of production of the solar ν_e. If this is above the resonance density $(N_e)^{res}_{1i}$ for the specific 12– or 13–flavor transition (*i.e.* $\nu_e \rightarrow \nu_\mu$ or $\nu_e \rightarrow \nu_\tau$), then $\theta^m_{1i} \rightarrow \frac{\pi}{2}$. Hence, the probability in (5) reduces to

$$
\langle P(\nu_e \rightarrow \nu_e)\rangle = P_1P_2c^2_{12}c^2_{13}+P_2(1-P_1)s^2_{12}s^2_{13}+(1-P_2)s^2_{13} \; , \tag{8}
$$

For large θ_{13}, the jump probabilities P_2 vanish (*i.e.* adiabatic approximation for 13–transitions), and we are left with

$$
\langle P(\nu_e \rightarrow \nu_e)\rangle = s^2_{13} \; , \tag{9}
$$

which is energy–independent (and, interestingly enough, independent of the 12–transitions). Conversely, the small θ_{13} limit of (8) is

$$
\langle P(\nu_e \rightarrow \nu_e)\rangle = c^2_{12}P_1P_2 \tag{10}
$$

which shows distinct energy dependence on both 12– and 13–flavor transitions. By studying the two limits in question, it is possible to see exactly how the third flavor affects the dynamics of the oscillation mechanism. The small θ_{13} solutions will in some respects approximate the two–flavor mechanism (which is fully recovered in the limit $\theta_{13} \rightarrow 0$). At the other extreme,

it is possible that the large θ_{13} solutions can yield spectral distortions which match observed ^8B fluxes, but cannot be obtained via the two–flavor model.

Since it was stated that the main difference between the VEP and MSW oscillation mechanisms should be visible in a study of the energy–dependent suppression of the neutrino flux, we show that striking differences can be observed for certain input parameters of the two models.

Although the ^8B decay is one of the rarest nuclear reactions in the Sun, the resulting ^8B neutrinos are the easiest to study, since they have the widest spectrum of $E \in [0, 15]$MeV, and are of sufficiently high energy to be observed by the ν_e-e scattering detectors (*e.g.* Kamiokande II, Superkamiokande, SNO). Hereafter, we provide a comparison of the ^8B flux curves as reduced by VEP and MSW, for both natural ($\Delta f_{31} > \Delta f_{21}, \Delta m^2_{31} > \Delta m^2_{21}$) and broken eigenvalue–hierarchies ($\Delta f_{31} < \Delta f_{21}, \Delta m^2_{31} < \Delta m^2_{21}$).

While chemical detectors can ascertain the rate of solar neutrinos which reach the Earth, the water–based detectors provide extra pieces of information which can help pin down parameters. An accurate measurement of the incident ^8B flux can tell us such things as which direction the neutrinos came from, exact arrival times (assuming they originate from the Sun) and, most importantly, show the energy–dependence of the suppression mechanism at work. Due to the fact that the Čerenkov detectors have relatively high energy thresholds, neutrinos whose energies are below these thresholds will not be visible. For example, KII has a threshold energy of $E_{th} = 9$ MeV [15], while SNO will have a lower one of $E_{th} \approx 5$ MeV. Thus, these experiments will be particularly useful if the parameter sets are such that suppression is visible in the high energy portion of the ^8B spectrum.

The (chemical detector) counting rate R^α for solar neutrinos from reaction–type α (*e.g.* ^8B, ^7Be decays, or the pp chain, hereafter ^8B, ^7Be, and pp neutrinos) is calculated via

$$R^\alpha = \int_0^{R_\odot} dr\, r^2 \xi^\alpha(r) \int_{E_{min}}^{E_{max}} dE\, \phi^\alpha(E) \sigma(E) \langle P(\nu_e \to \nu_e) \rangle (r, E)\ , \qquad (11)$$

where $\sigma(E)$ is the detector–material absorption cross–section for neutrinos, $\phi^\alpha(E)$ the unreduced neutrino flux [15], and $\xi^\alpha(r)$ the fractional neutrino production rate at radius r [5]. Note that the size of the flux curve does not reflect the resulting counting rate, so much as does its *shape*. The counting

rate in eq.(11) is essentially calculated as

$$R^{\alpha} = \sum_{i} \phi_i^{\alpha} \sigma_i \ , \tag{12}$$

and so the same R can be obtained for small fluxes as well as for large ones, since the cross–section $\sigma_i \equiv \sigma(E)$ increases with increasing energy. It is the location of the unsuppressed curve on the energy–axis which determines this. We have performed a numerical integration of Eq. (11) using the SSM data mentioned in the previous paragraph. Figures 1–5 show both MSW– and VEP–reduced ^8B fluxes for various allowed counting rates, as compared with the SSM (unreduced) flux of $\Phi^{^8B}_{SSM} = 5.8 \times 10^6 \mathrm{cm}^{-2}\ \mathrm{s}^{-1}$. All mass–differences Δm^2_{i1} are expressed in units of eV^2.

The effects of the MSW/VEP mechanisms on solar neutrino depletion hinge on the existence of a matter–induced flavor–conversion resonance between different neutrinos (*e.g.* $\nu_e \rightarrow \nu_\mu$). There are three possible resonances for three flavors: $\nu_e \rightarrow \nu_\mu$, $\nu_e \rightarrow \nu_\tau$, $\nu_\mu \rightarrow \nu_\tau$ (and vice versa). For solar neutrinos, we are only concerned with flavor conversion from $\nu_e \rightarrow \nu_x$, where ν_x is either of the other two flavors.[2] Resonances can occur if the ν_es are created at an electron density $(N_e)^{cr} > (N_e)^{res}_{1i}$, with $i = 2, 3$ for the other two flavors, where

$$(N_e)^{res}_{1i} = \frac{1}{G_F} \sqrt{2} |\phi(r)| \Delta f E \cos 2\theta_{1i} \tag{13}$$

For MSW, simply make the substition in eq. (7), and replace mass–eigenstate vacuum mixing angles with gravitational ones.

Conversely, if $(N_e)^{cr} < (N_e)^{res}_{1i}$, the ν_e will never undergo resonance, and will propagate as if in vacuum. We consider here only the case $(N_e)^{res}_{1i} > (N_e)_{max}$, *i.e.* the ν_e resonance density exceeds the maximal solar electron density. We refer to this behavior according to the following: single resonance ($(N_e)^{cr} > (N_e)^{res}_{1i}$ for $i = 2$ *or* 3 only), and double resonance ($(N_e)^{cr} > (N_e)^{res}_{1i}$ for both $i = 2, 3$).

We note a marked difference between small and large angle solutions. Essentially, the large–angle solutions show very little variation in the fluxes. This is consistent with the form of (9), which show the ν_e–attenuation to be energy independent. The least variation is visible in the double–resonance

[2]We do not consider arbitrary sterile neutrinos in this analysis.

case (fig. 1), while we see more of a discrepancy in the models for a single–resonance (for both natural– and broken–hierarchies, figs 2, 3). This difference is mostly in the low–energy neutrinos, though, and so would be difficult to detect. The curves for large θ_{12}, small θ_{13} show similar energy independence, and thus are not presented here.

In contrast, the small–angle solution shows very different behaviour. Figure 4 depicts the double–resonance reduced ^8B neutrino flux for the two models, with quite surprising dissimilarities. The two models show *opposite* energy–dependent reduction: MSW suppresses low energy neutrinos, while VEP suppresses high energy ones[3]. Furthermore, the broken hierarchy case for the small angle region (fig. 5) shows other intriguing behavior. As mentioned earlier, the counting rate is determined by the product of the cross–section $\sigma(E)$ and the flux $\phi(E)$. Here we see an example of where both large and small fluxes can represent the same counting rate. Whereas the natural hierarchy attenuated low energy neutrinos, here we see that the situation is reversed: the large curve shows the low–energy neutrinos largely uneffected by the MSW mechanism, while VEP leaves high–energy neutrinos alone.

This radically different spectral distortion between the two models can in part be explained by the fact that (especially for small mixing angles) the adiabatic and non–adiabatic transitions are reversed. It is noted in [10] that the adiabaticity condition is violated for low energy neutrinos in VEP, while it is violated for high energy neutrinos in MSW. This is clearly reflected in the small θ_{13} solutions of figs. 4, 5.

In summary, the inclusion of a third flavor in each mechanism yields a widely varying range of possible flux curves depending upon the values of the mixing angle parameters. The small angle solution offers variations in the structure of $\langle P(\nu_e \to \nu_e)\rangle$, while still approximating the two–flavor limit ($\theta_{13} \to 0$). In the case of the small 13–mixing region for double flavor–resonances, the flux suppression is opposite for the two mechanisms. For an unbroken hierarchy, the VEP mechanism attenuates low energy neutrinos whereas MSW attenuates the higher energy range; in the case of a broken hierarchy the roles played by each mechanism are interchanged. The large θ_{13} solutions are energy independent, thus making it difficult to distinguish between MSW and VEP in the high–energy portion of the spectrum, as most

[3]The rough nature of the curves is attributed to numerical variations, and most likely not a physical behavior.

spectral distortions occur here toward the lower end. Additional information from atmospheric observations [16] and laboratory experiments [17] will then be essential in determining the underlying oscillation mechanism.

Acknowledgements

This work was supported in part by the Natural Sciences and Engineering Research Council of Canada.

References

[1] R. Davis, D. S. Harmer, and K. C. Hoffman, Phys. Rev. Lett. **20**, 1205 (1968).

[2] Kamiokande II Collaboration, K. Hirata *et al.*, Phys. Rev. Lett. **65**, 1297 (1990).

[3] GALLEX Collaboration, P. Anselmann *et al.*, Phys. Lett. **B327**, 377 (1994).

[4] SAGE Collaboration, J. N. Abdurashidov *et al.*, Phys. Lett. **B328**, 234 (1994).

[5] J. N. Bahcall and M. H. Pinsonneault, Rev. Mod. Phys. **64**, 885 (1992).

[6] S. P. Mikheyev and A. Yu. Smirnov, Yad. Fiz. **42**, 1441 (1985).

[7] S. P. Mikheyev and A. Yu. Smirnov, Phys. Lett. **B21**, 560 (1988).

[8] L. Wolfenstein, Phys. Rev. **D17**, 2369 (1978).

[9] M. Gasperini, Phys. Rev. **D38**, 2635 (1988).

[10] J. N. Bahcall, P. I. Krastev, and C. N. Leung, IASSNS-AST 94/54, UDHEP-10-94 (October 1994); for earlier work see M. N. Butler *et al.*, Phys. Rev. **D47**, 2615 (1993); A. Halprin and C. N. Leung, Phys. Rev. Lett. **67**, 1833 (1991); J. Pantaleone, A. Halprin, and C. N. Leung, Phys. Rev. **D47**, R4199 (1993); K. Iida, H. Minakata and O. Yasuda, Mod. Phys. Lett. **A8** (1993) 1037.

[11] H. Minakata and H. Nunokawa, KEK-TH-396/TMUP-HEL-9402, (hep-ph 9405239) (April 1994).

[12] A. Baldini and G. F. Giudice, Phys. Lett. **B186**, 211 (1987).

[13] J. Mureika, *Gravitationally–Induced Three–Flavor Neutrino Oscillations as a Possible Explanation of the Solar Neutrino Problem*, M.Sc. thesis, University of Waterloo (1995).

[14] H. W. Zaglauer and K. H. Schwarzer, Phys. Lett. **B198** 556 (1987).

[15] J. N. Bahcall, *Neutrino Astrophysics*, Cambridge University Press, 1988.

[16] M.C. Goodman, Nucl. Phys. **B38** (Proc. Supp.) (1995) 337; K.S. Hirata *et. al.*, Phys. Lett. **B280** (1992) 146; D. Casper *et.al.* Phys. Rev. Lett. **66** (1991) 2561.

[17] L. Borodovsky *et. al.*, Phys. Rev. Lett. **68** (1992) 274; V.V. Ammosov *et. al.*, Z. Phys. **C40** (1988) 487. C. Athanassopoulos *et. al.*, Phys. Rev. Lett. **75** (1995) 2650; J. Hill, Phys. Rev. Lett. **75**, (1995) 2654; B.T. Cleveland *et. al.* Nucl. Phys. **B38** (Proc. Supp.) (1995) 47.

Figure Captions All captions list parameters used to obtain the reduced counting rate R. Neutrino masses are expressed in units of eV^2.

Fig. 1: $\Delta f_{21} = 10^{-15}$, $\Delta f_{31} = 4 \times 10^{-14}$; $\Delta m^2_{21} = 6.15 \times 10^{-6}$, $\Delta m^2_{31} = 5 \times 10^{-5}$;

Fig. 2: $\Delta f_{21} = 10^{-15}$, $\Delta f_{31} = 4 \times 10^{-14}$; $\Delta m^2_{21} = 6.15 \times 10^{-6}$, $\Delta m^2_{31} = 5 \times 10^{-5}$;

Fig. 3: $\Delta f_{21} = 10^{-8}$, $\Delta f_{31} = 3 \times 10^{-14}$; $\Delta m^2_{21} = 10^{-1}$, $\Delta m^2_{31} = 6 \times 10^{-5}$;

Fig. 4: $\Delta f_{21} = 2.7 \times 10^{-15}$, $\Delta f_{31} = 10^{-14}$; $\Delta m^2_{21} = 10^{-5}$, $\Delta m^2_{31} = 1.6 \times 10^{-4}$;

Fig. 5: $\Delta f_{21} = 10^{-8}$, $\Delta f_{31} = 1.31 \times 10^{-14}$; $\Delta m^2_{21} = 10^{-1}$, $\Delta m^2_{31} = 1.31 \times 10^{-4}$;

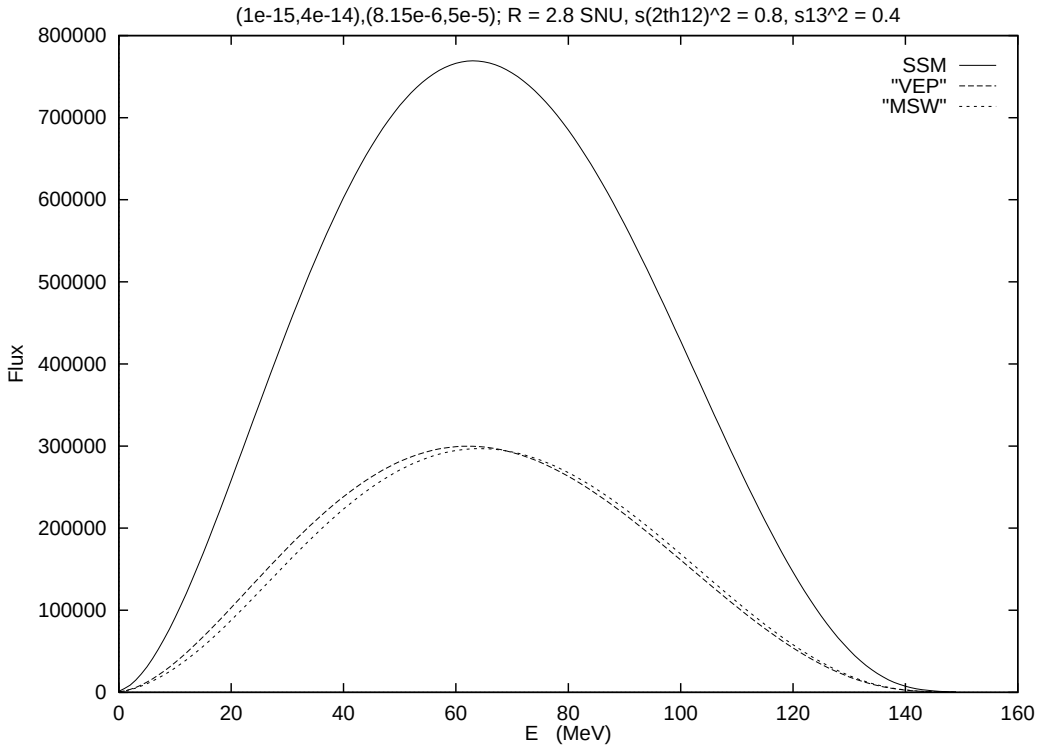
(1e-15,4e-14),(8.15e-6,5e-5); R = 2.8 SNU, s(2th12)^2 = 0.8, s13^2 = 0.4
SSM
"VEP"
"MSW"
Flux
E (MeV)
0
100000
200000
300000
400000
500000
600000
700000
800000
0
20
40
60
80
100
120
140
160

Figure 1:

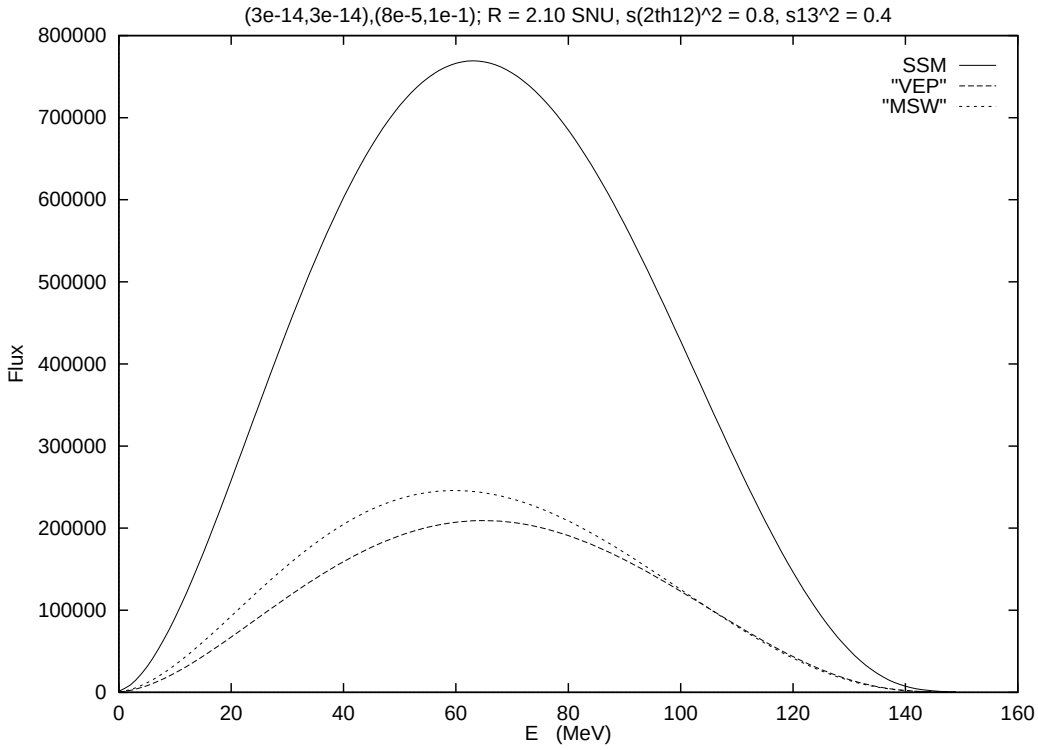
(3e-14,3e-14),(8e-5,1e-1); R = 2.10 SNU, s(2th12)^2 = 0.8, s13^2 = 0.4
SSM
"VEP"
"MSW"
Flux
E (MeV)
0
100000
200000
300000
400000
500000
600000
700000
800000
0
20
40
60
80
100
120
140
160

Figure 2:

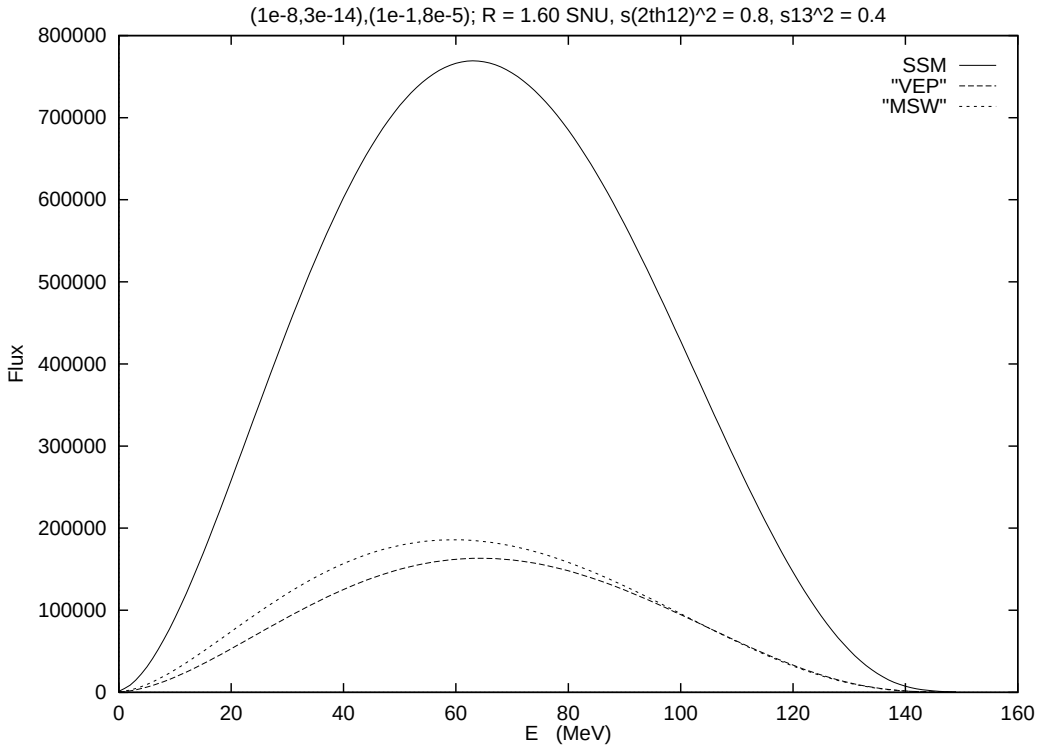
(1e-8,3e-14),(1e-1,8e-5); R = 1.60 SNU, s(2th12)^2 = 0.8, s13^2 = 0.4
SSM
"VEP"
"MSW"
Flux
E (MeV)
0
100000
200000
300000
400000
500000
600000
700000
800000
0
20
40
60
80
100
120
140
160

Figure 3:

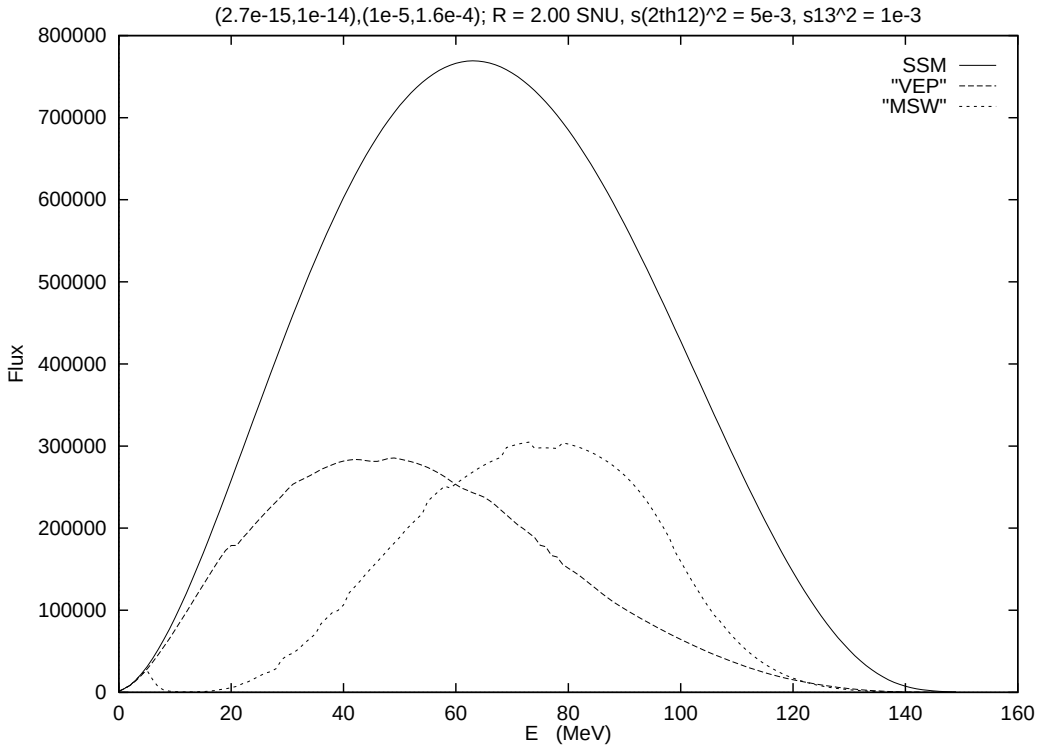
(2.7e-15,1e-14),(1e-5,1.6e-4); R = 2.00 SNU, s(2th12)^2 = 5e-3, s13^2 = 1e-3
SSM
"VEP"
"MSW"
Flux
E (MeV)
0
100000
200000
300000
400000
500000
600000
700000
800000
0
20
40
60
80
100
120
140
160

Figure 4:

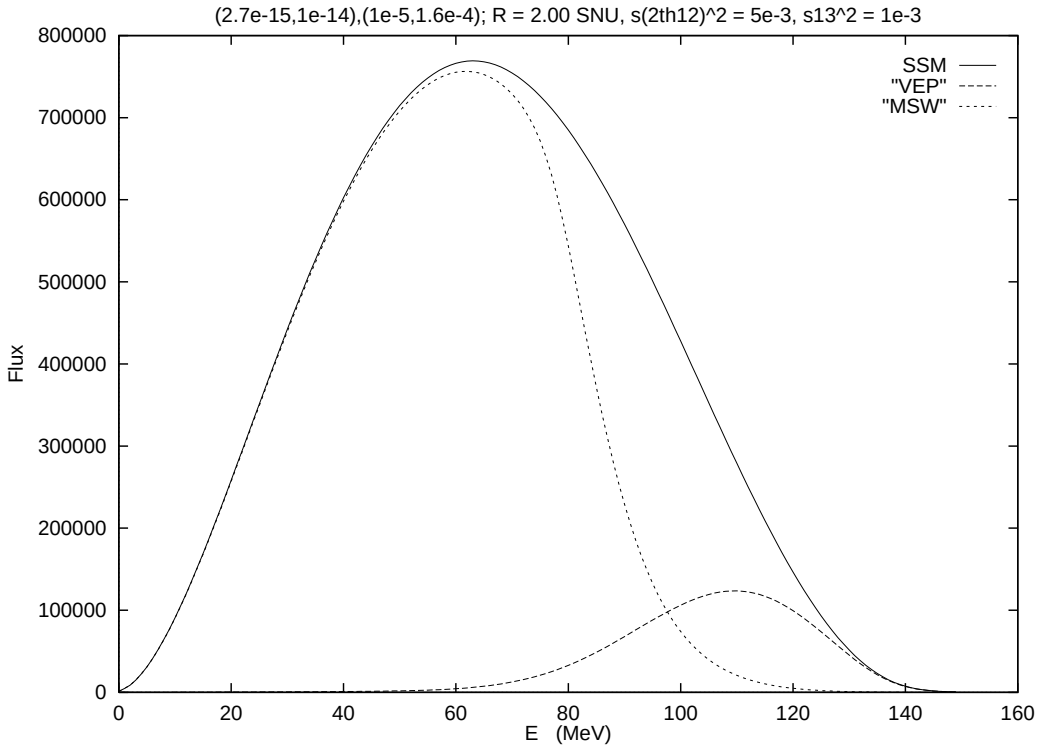
(2.7e-15,1e-14),(1e-5,1.6e-4); R = 2.00 SNU, s(2th12)^2 = 5e-3, s13^2 = 1e-3
SSM
"VEP"
"MSW"
Flux
E (MeV)
0
100000
200000
300000
400000
500000
600000
700000
800000
0
20
40
60
80
100
120
140
160

Figure 5: